Supporting Information

Two p-type ester-linked dihydrophenazine-based polymers as high-performance cathode materials for lithium-ion batteries

Jingying Guo, [a] Xiangling Peng, [a] Bo Ouyang, [a] Dong Huang, [a] Zerong Jing, [b] Xinhang Bian, [a] Ya Du [b] and Haishen Yang *[a]

a. Shanghai Key Laboratory of Materials Protection and Advanced Materials in Electric Power, College of Environmental and Chemical Engineering, Shanghai University of Electric Power, Shanghai 200090, China. E-mail: yanghsh@shiep.edu.cn

b. Institute if Advanced Synthesis, School of Chemistry and Molecular Engineering, Nanjing Tech University, Nanjing 211816, China. E-mail: ias_ydu@njtech.edu.cn

Reagents

All chemicals used in the synthesis were purchased from commercial suppliers and used without further purification. Phenazine (PNZ, 98%), methyltributylammonium chloride (MTBAC, 99%), acetonitrile (MeCN, 99.9%), 2-bromoethanol (C_2H_5BrO, 98%), *N,N'*-carbonyl diimidazole (CDI, 98%), trimesoyl chloride (TMC, 98%), pyridine (C_5H_5N, 99.5%), N,N-dimethylacetamide (DMAc, 99.8%), N,N-dimethylformamide (DMF, 99.8%), Tetrahydrofuran (THF, 99.9%), N-Methylpyrrolidone (NMP, 99.5%), Trichlorobenzene ($C_6C_3Cl_3$, 99%) were purchased from Adamas; sodium dithionite ($Na_2S_2O_4$, ≥ 88%), methanol (CH_3OH, 99.5%), dimethyl sulfoxide (DMSO, 99%), acetone (C_3H_6O, 99.5%) were purchased from Greagent; sodium carbonate (Na_2CO_3, 99.5%) was purchased from Macklin; chloroform ($CHCl_3$, ≥99.0%) was purchased from Shanghai trial brand.

Materials characterizations

Proton nuclear magnetic resonance (^{1}H NMR) spectrum was acquired on a Bruker AVANCE III 400M. Fourier transform infrared (FT-IR) spectra were obtained from PerkinElmer Spectrum Two FT-IR with a range from 400 to 4000 cm^{-1}. Scanning electron microscopy (SEM) images were detected on JEOL JSM-7810F. Thermogravimetric analysis (TGA) was measured on the NETZSCH STA 409 PC/PG apparatus in a wide temperature range of 30-600 °C with a heating rate of 10 °C min^{-1} under nitrogen atmosphere. X-ray diffraction (XRD) patterns were gained on Smartlab3KW.

Materials preparation

*Synthesis of 5,10-bis(2-hydroxyethyl)phenazine (**BHEP**)*.[1] Phenazine (3.60 g, 20 mmol), sodium dithionite (5.218 g, 30 mmol), sodium carbonate (4.235 g, 40 mmol), methyltributylammonium chloride (1.885 g, 8 mmol) were placed into a 500 mL two-necked round-bottom flask. Then, acetonitrile (40 mL), deionized water (10 mL), and 2-bromoethanol (14.979 g, 120 mmol) were added to the flask. The reaction mixture was stirred at 100 °C and refluxed for 48 h. After the reaction was completed, water (100 mL) was added dropwise to the reflux reaction

system and then cooled to room temperature. The green needle-like crystals (5.080 g in 94.03% yield) were obtained by filtration and dried in a vacuum at 100 °C. ^{1}H NMR (400 MHZ, DMSO-d_6): δ 4.92 (s, 2H), 3.56 (q, 8H).

*Synthesis of poly(5,10-phenazinediethanol carbonate) (**PPDC**)*. **BHEP** (0.3 g, 1.110 mmol) and *N,N'*-carbonyl diimidazole (0.202 g, 1.221 mmol) were added in a 25 mL tube-type Schlenk flask, respectively. Then 1.5 mL acetonitrile was added under nitrogen environment. After stirring at 90 °C for 48 h, *N,N'*-carbonyl diimidazole (0.202 g, 1.221 mmol) and 1 mL acetonitrile were added to the reaction system to continue stirring at 90 °C for 24 h. Finally, the product was washed with water, methanol, dimethyl sulfoxide, and acetone until it was clear. The light brown pink solid product (225.1 mg in 68% yield) was vacuum dried at 80 °C.

*Synthesis of poly(5,10-phenazine diethanol-1,3,5-tribenzoate) (**PPTC**)*. **BHEP** (0.2 g, 0.740 mmol) was added in a 25 mL tube-type Schlenk flask. Then 1.5 mL pyridine was added under nitrogen environment and stirred until **BHEP** was completely dissolved. Trimesoyl chloride (0.134 g, 0.500 mmol) was added at 0 °C, stirred for 5 min and then stirred at room temperature for 24 h. Finally, the product was washed with water, *N,N*-dimethylacetamide, and methanol until the solution was clear. The orange solid product (135.7 mg in 50% yield) was vacuum dried at 80 °C.

Electrochemical measurements

Electrochemical measurements were performed using a standard CR-2016 coin-type half-cells which consist of a working electrode, Celgard 2400 membrane, nickel foam, and stainless steel positive and negative shells. To prepare working electrodes, a slurry containing 50% of active materials (**PPDC** or **PPTC**), 40% of conductive additives (multi-walled carbon nanotubes, MWCNTs) and 10% of binder (polyvinylidene fluoride, PVDF) in *N*-methylpyrrolidone (NMP) was homogenized by ball milling at room temperature for 2 h. Then, the electrode composite was coated on the surface layer of the aluminum foil, dried in vacuum at 80 °C for 12 h. The dried materials were cut into circular electrodes (D = 14 mm) for assembly into coin cells. The CR-2016 coin cells were assembled in the glove box (H_2O < 0.01 ppm, O_2 < 0.01 ppm), select 1 M $LiPF_6$ in EC/DEC (v/v=1:1) as electrolyte for **PPDC** battery or 1 M $LiPF_6$ in EC/DEC/DMC (v/v/v=1:1:1) as electrolyte for **PPTC** battery, and metallic lithium as the anode. The galvanostatic charge/discharge tests were performed in a voltage range of 2.0-4.3 V vs. Li/Li^+ for **PPDC** battery (or a voltage range of 2.0-4.2 V vs. Li/Li^+ for **PPTC** battery) on the NEWARE CT-4008 cell test instrument (Shenzhen, China). When the electrolyte is 1 M LiTFSI-DOL/DME (v/v=1:1), both **PPDC** and **PPTC** batteries were performed in a voltage range of 1.2-3.9 V at galvanostatic charge/discharge test. Electrochemical cyclic voltammetry (CV) and electrochemical impedance spectroscopy (EIS) were both recorded on electrochemical workstation system (PGSTAT302N Autolab, Metrohm, Switzerland). All the electrochemical tests were performed at room temperature. Identification of surface capacitive effect and diffusion-controlled insertion process. The mathematic relation between peak current (*i*) and scan rate (*v*) of the sweep-rate-dependent cyclic voltammetry (CV) curves can be expressed as follows：

$$\mathrm{a} = iv^b \qquad (1)^2$$

Among them， a and b are the parameters. When the b value approaches to 0.5, it indicates that the reaction is limited by diffusion controlled processes, and the b value approaches to 1, it indicates the reaction is limited by capacitive controlled lithium reaction processes. Furthermore, to quantify the diffusion- and capacitive-controlled contributions to the cathode capacity, the current is divided into two part, diffusion ($k_2v^{1/2}$) and capacitance (k_1v), respectively, according to the following equation:

$$i = k_1 v + k_2 v^{1/2} \quad (2)^3$$

It's possible to quantify the fraction of the current due to each of these contributions at specific potentials by determining k_1 and k_2, which could be obtained from the plot of $i/v^{1/2}$ vs. $v^{1/2}$.

Supporting Figures

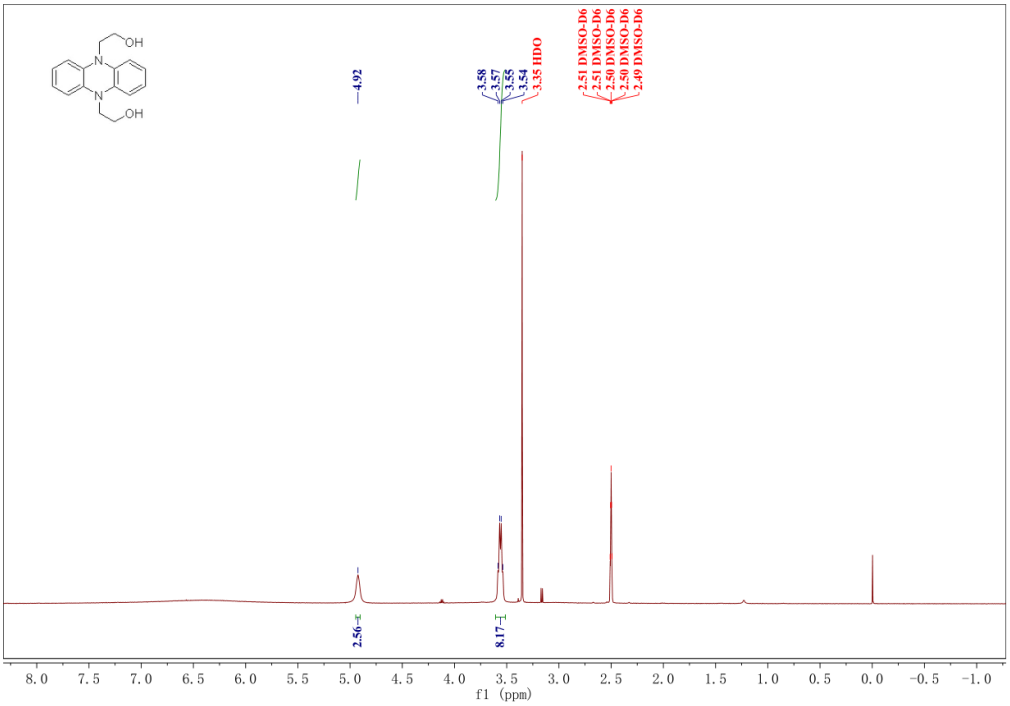

Fig. S1 ^{1}H NMR spectrum of **BHEP** in DMSO-d_6.

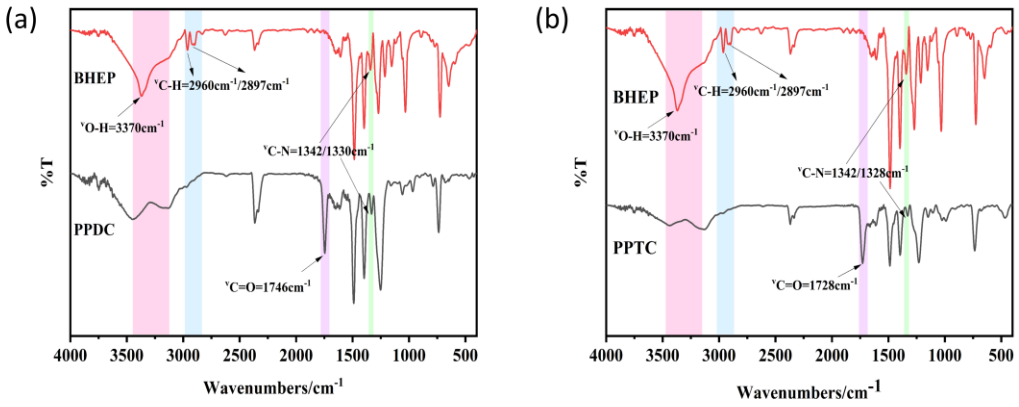

Fig. S2 FT-IR spectra of (a) **PPDC**; (b) **PPTC**.

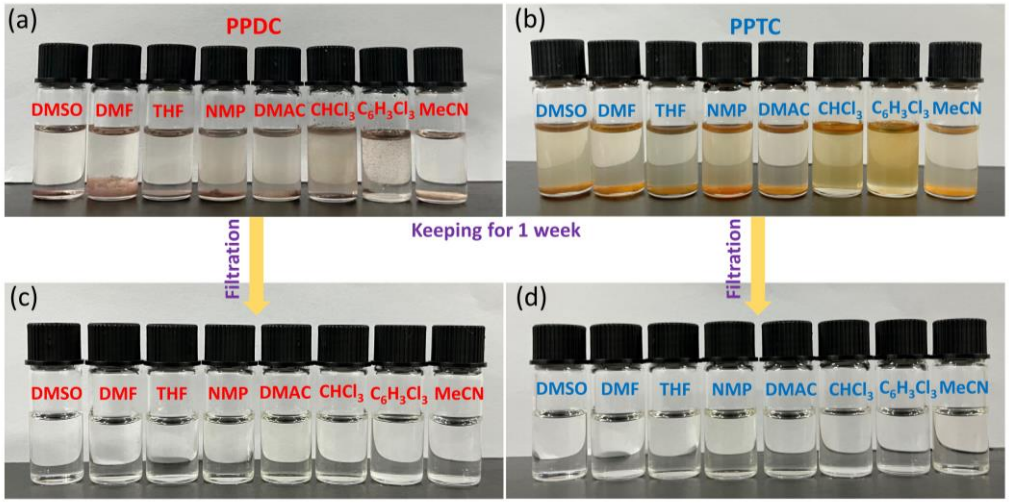

Fig. S3 The pictures of (a and c) **PPDC** and (b and d) **PPTC** in common organic solvents, and the corresponding filtrates. 2 mg of **PPDC** (or **PPTC**) samples were added to a vial containing 1 mL of DMSO, DMF, THF, NMP, DMAc, $CHCl_3$, $C_6H_3Cl_3$, and MeCN solvents, respectively. After standing for 1 week, the mixtures were filtered to obtain clear filtrates.

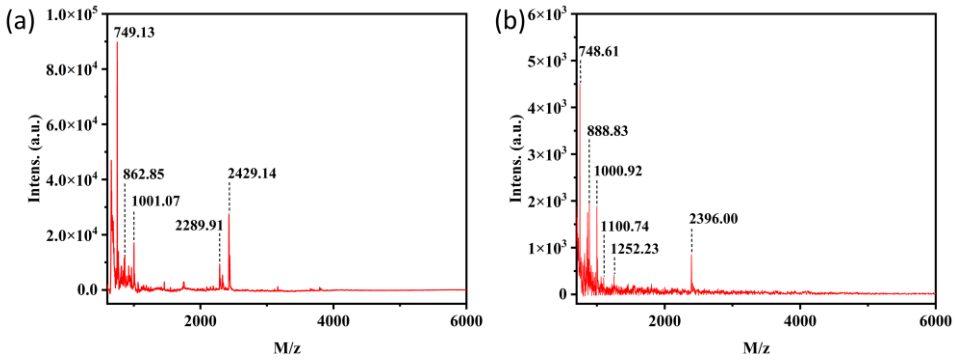

Fig. S4 MALDI-TOF Mass spectrum of (a) **PPDC**; (b) **PPTC**.

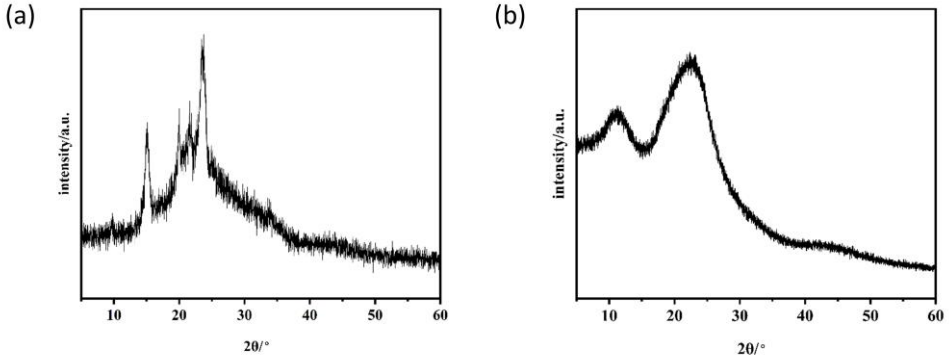

Fig. S5 XRD pattern of (a) **PPDC**; (b) **PPTC**.

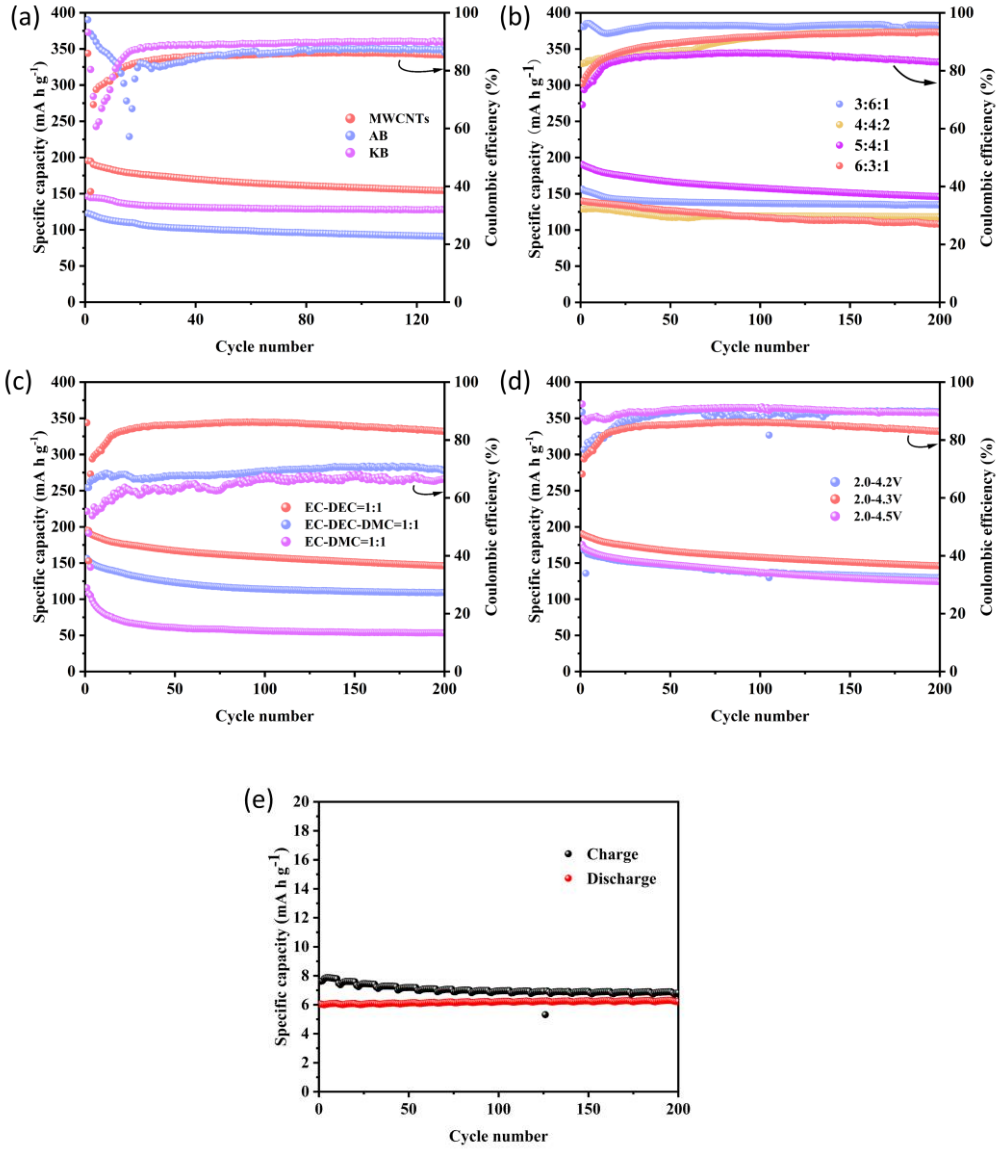

Fig. S6 The electrochemical performance of **PPDC** at 0.2 A g^{-1}. (a) different conductive carbon materials; (b) different composite ratios; (c) different electrolytes; (d) different voltage ranges; (e) capacity contribution of MWCNTs at 2.0-4.3 V.

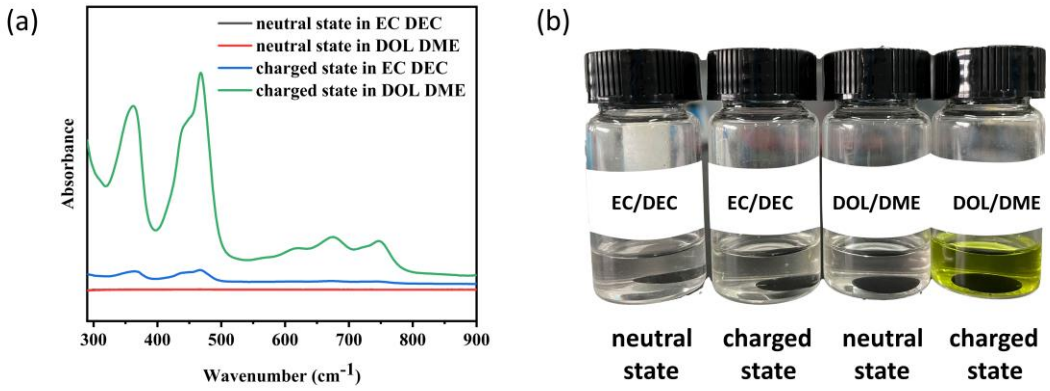

Fig. S7 PPDC electrode sheets of neutral and fully charged states were removed from the batteries, and then were immersed in electrolytes for 1 h. (a) UV-Vis spectra of **PPDC** electrodes in EC/DEC and DOL/DME solutions: neutral and charged states; (b) Color Phenomena of **PPDC** electrodes in EC/DEC and DOL/DME solutions: neutral and charged states: the solutions containing neutral **PPDC** electrodes appear colorless in both EC/DEC and DOL/DME solvents; the solutions with charged **PPDC** electrodes exhibit a very faint yellow color in EC/DEC and a yellowish green hue in DOL/DME solvents.

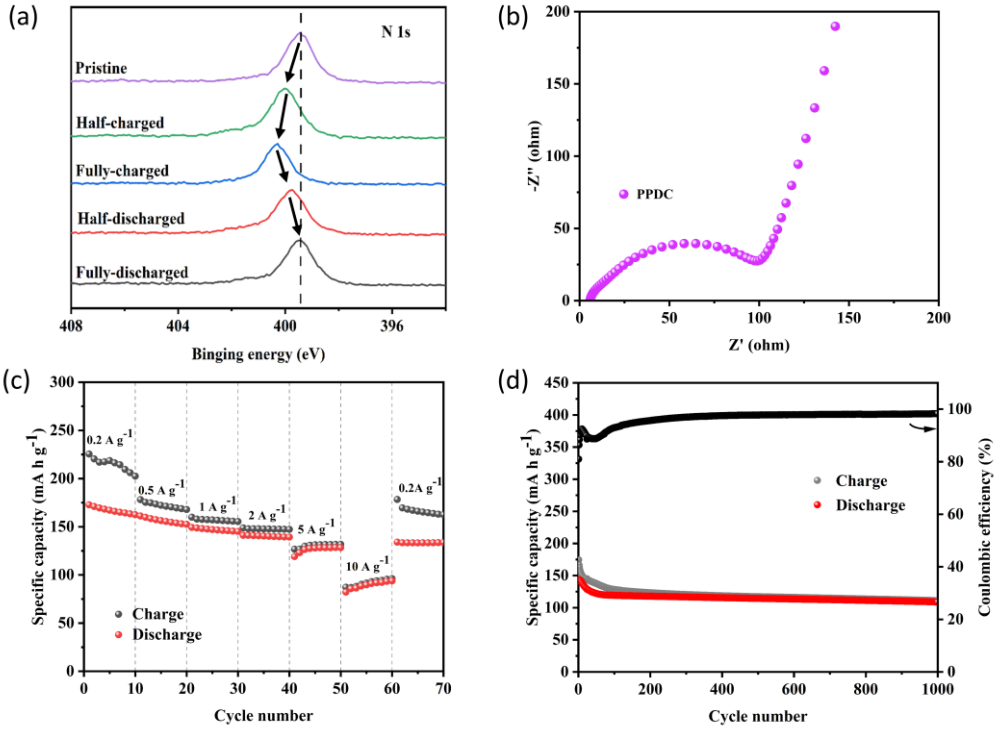

Fig. S8 (a) XPS characterization of N 1s region; (b) Electrochemical impedance spectra (EIS); (c) Rate capability; (d) Cycling stability at 1 A g^{-1} for **PPDC**.

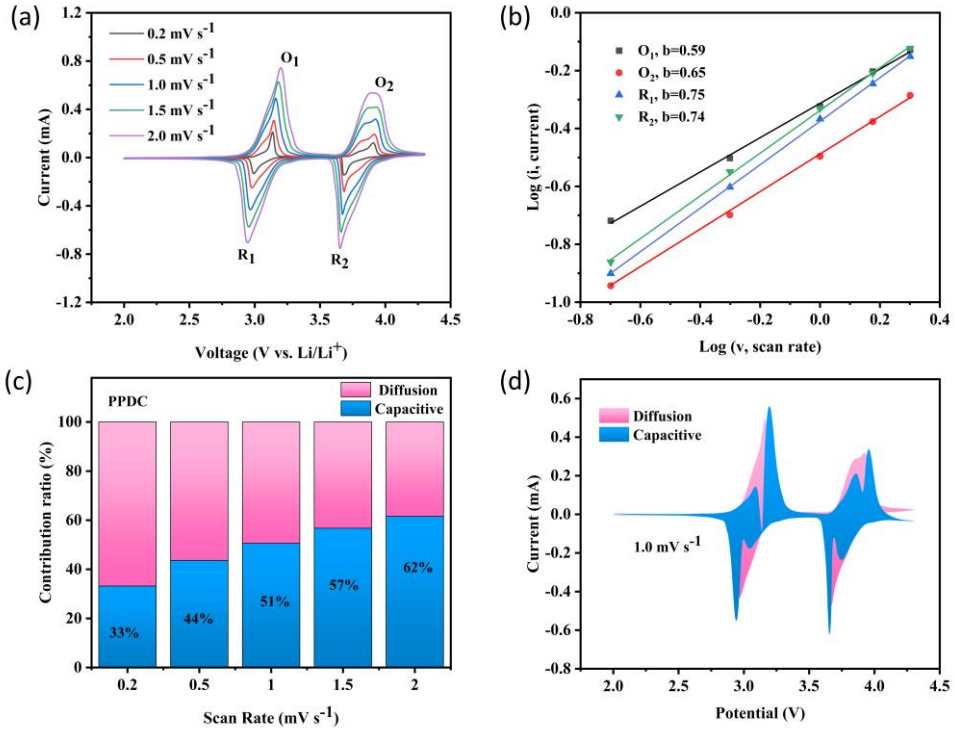

Fig S9 (a) The CV curves of **PPDC** at different scan rates. (b) The fitted lines between log (*i*) and log (*v*) of **PPDC**. (c) The capacity contribution of **PPDC** at different scan rates. (d) The capacity contribution of PPDC at 1.0 mV s^{-1}.

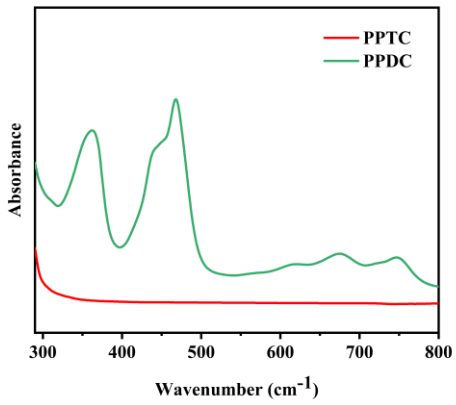

Fig. S10 PPDC and **PPTC** electrode sheets of fully charged states were removed from the batteries, and then were immersed in electrolytes for 1 h. UV-Vis spectra of charged state of **PPTC** and **PPDC** in DOL/DME.

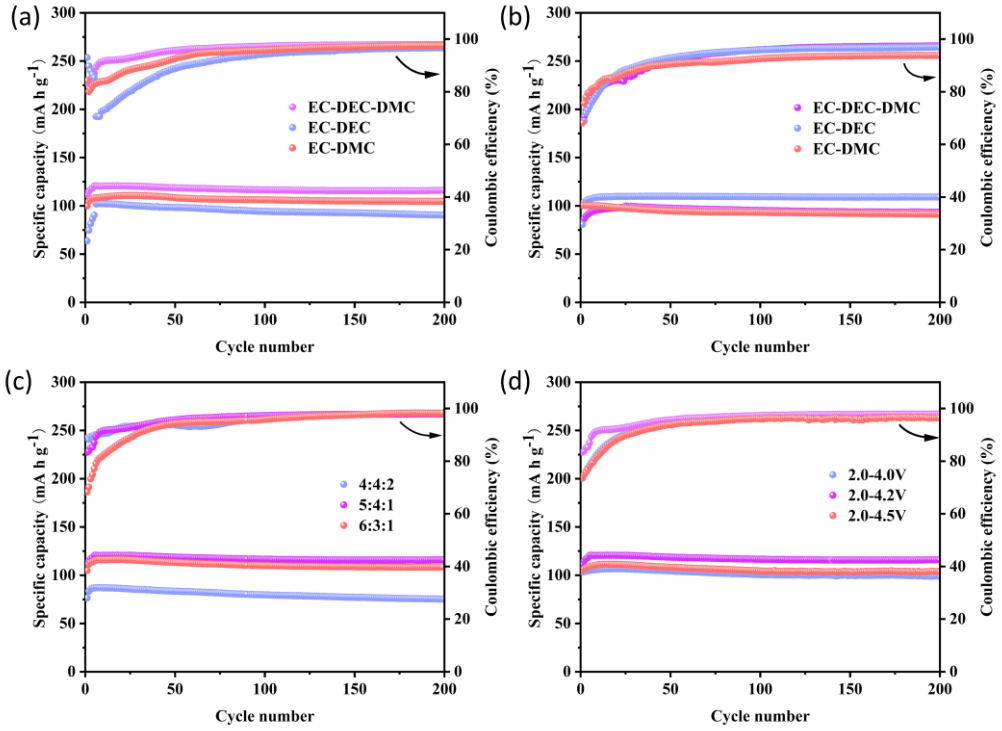

Fig. S11 The electrochemical performance of **PPTC** at 0.2 A g^{-1} in three kinds of electrolytes using two different carbon agents. (a) Multi-walled carbon nanotubes (MWCNTs); (b) Acetylene black (AB); (c) Different electrolytes; (d) Different voltage ranges.

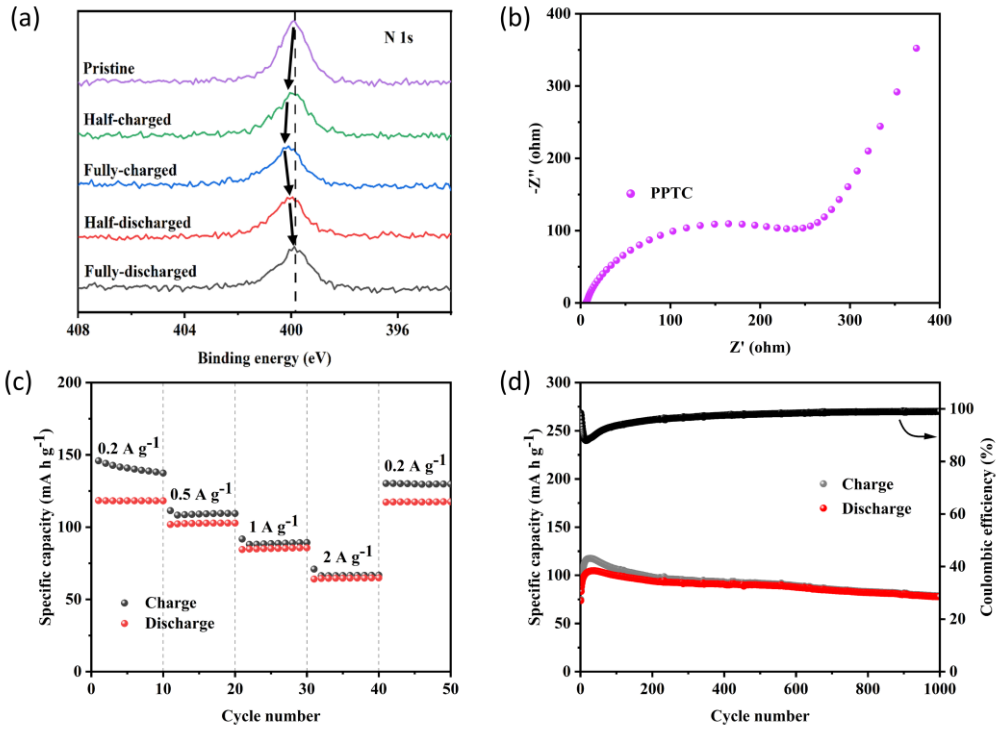

Fig. S12 (a) XPS characterization of N 1s region; (b) Electrochemical impedance spectra (EIS); (c) Rate capability; (d) Cycling stability at 1 A g^{-1} for **PPTC**.

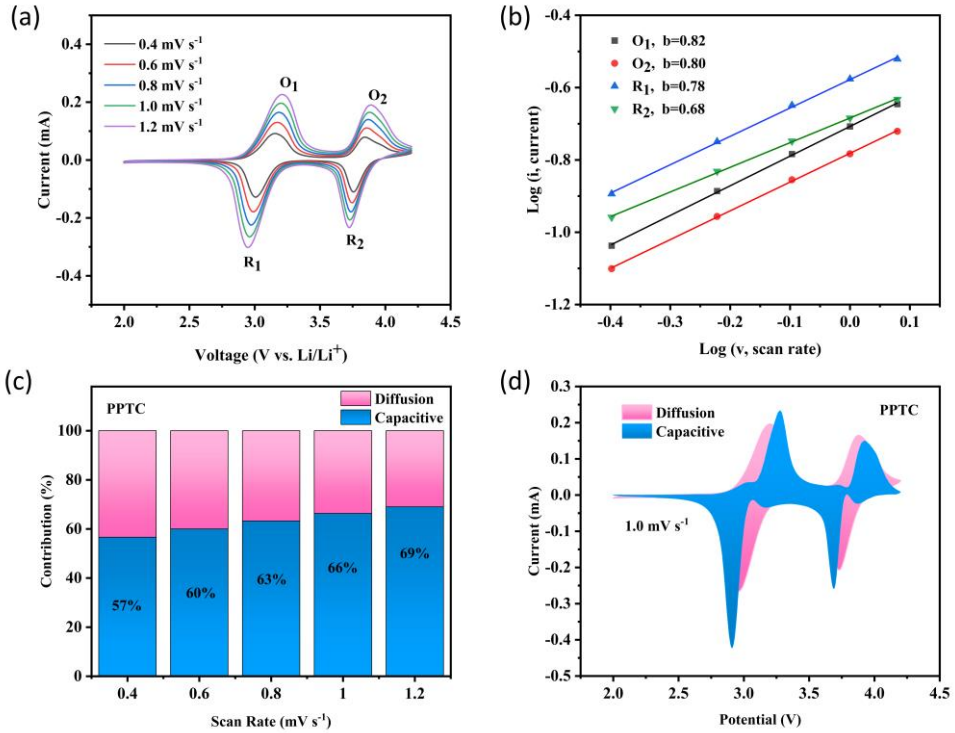

Fig S13 (a) The CV curves of **PPTC** at different scan rates. (b) The fitted lines between log (*i*) and log (*v*) of **PPTC**. (c) The capacity contribution of **PPTC** at different scan rates. (d) The capacity contribution of **PPTC** at 1.0 mV s^{-1}.

Table S1 The spectroscopy results for N1s peaks of **PPDC** and **PPTC** with those of reported organic DHPs cathodes.

DHPs cathodes	Pristine (eV)	half-charged (eV)	fully-charged (eV)	half-discharged (eV)	fully-discharged (eV)
PPDC (this work)	399.45	400.03	400.28	399.72	399.45
PPTC (this work)	400.04	400.32	400.51	400.32	400.04
PMEPZ[4]	398.98	399.48	399.78	399.48	398.98
p-TPZB[5]	399.8	400.1	401.2	400.1	399.9
PBEMP[6]	399.38	399.58	399.78	399.58	399.38
PyPz[7]	400.2	/	400.4	/	400.2
DPZPC[8]	399.5	/	401.3	/	399.5

Table S2. The comparison of electrochemical performances of **PPDC** and **PPTC** with those of leading anion-hosting organic cathodes in recent investigations.

Cathode materials	Charge carrier	Theoretical capacity (mA h g^{-1})	Initial capacity (mA h g^{-1})	capacity retention (cycle number, current)	Rate capacity (mA h g^{-1}) (current)	Ref.
PPDC	PF_6^-	181	180	78% (200, 0.2 A g^{-1})	82 (10 A g^{-1})	this
PPTC	PF_6^-	143	120	97% (200, 0.2 A g^{-1})	64 (2 A g^{-1})	work
PyPz	$AlCl_4^-$	239	/	94% (1000, 0.2 Ag^{-1})	116 (30 A g^{-1})	7[7]
PVDMP	PF_6^-	227	220	68% (3900, 5 C)	131 (20 C)	9[9]
PTMA-filled NCNTs	PF_6^-	222	160	80% (3000, 1 C)	90 (20 C)	10[10]
PhPz	$AlCl_4^-$	210	/	75% (1000, 0.2 Ag^{-1})	61 (30 A g^{-1})	7[7]
p-DPPZ	PF_6^-	209	145	89% (500, 1 C)	65 (5 C)	11[11]
p-PZ	PF_6^-	209	198	92% (800, 0.5 C)	80 (10 C)	12[12]
PDPAPZ	PF_6^-	209	117	86% (100, 5 A g^{-1})	82 (20 A g^{-1})	13[13]
PDPPD	PF_6^-	209	/	77% (500, 0.5 C)	53 (200 C)	14[14]
BPyPz	ClO_4^-	206	205	89% (300, 05 C)	126 (20 C)	15[15]
CPP	PF_6^-	204	184	92% (500, 0.2 A g^{-1})	156 (1 A g^{-1})	16[16]

P3-based	ClO_4^-	204	133	85% (200,.1 C)	150 (100 C)	17[17]
DPZPC	ClO_4^-	191	184	84% (400, 0.1 A g^{-1})	126 (1 A g^{-1})	8[8]
DPZPA	ClO_4^-	190	138	82% (400, 0.1 A g^{-1})	100 (1 A g^{-1})	8[8]
NCPP	PF_6^-	185	149	54% (500, 0.2 A g^{-1})	81 (1 A g^{-1})	16[16]
p-TPZB	PF_6^-	174	155	89% (2000, 2 C)	120 (10 C)	5[5]
p-DPPZR1	PF_6^-	150	146	95% (800, 1 C)	120 (10 C)	18[18]
p-DPPZS	PF_6^-	147	133	90.2% (1000, 5 C)	64 (20 C)	19[19]
P3	ClO_4^-	144	53	59 (250, 1 C)	77 (1 C)	20[20]
TzPz	PF_6^-	140	192	99% (400, 0.2 A g^{-1})	108 (30 A g^{-1})	21[21]
BzPz	PF_6^-	140	148	79% (400, 0.2 A g^{-1})	44 (30 A g^{-1})	21[21]
PVK	PF_6^-	138	104	70% (400, 0.5 A g^{-1})	68 (2 A g^{-1})	22[22]
PBEMP	PF_6^-	132	123	92% (200, 0.2 A g^{-1})	111 (1.6 A g^{-1})	6[6]
3PXZ	$TFSI^-$	129	73	65% (100, 1 C)	76 (20 C)	23[23]
p-DPICZ-O	PF_6^-	125	90	87% (800, 1C)	49 (10 C)	24[24]
PVMPT	PF_6^-	112	50	93.5% (10000, 10 C)	26 (100 C)	25[25]
TCTA	PF_6^-	/	80	60% (5000, 1 A g^{-1})	38 (20 A g^{-1})	26[26]
Coronene	PF_6^-	/	40	92% (960, 0.02 A g^{-1})	21 (0.5 A g^{-1})	27[27]

1. J. R. Lomprey, T. F. Guarr, K. L. Baumann and P. Giri, *US06445486 B1*, 2002.
2. H. Lindström, S. Södergren, A. Solbrand, H. Rensmo, J. Hjelm, A. Hagfeldt and S.-E. Lindquist, *The Journal of Physical Chemistry B*, 1997, **101**, 7717-7722.
3. T. C. Liu, W. G. Pell, B. E. Conway and S. L. Roberson, *Journal of The Electrochemical Society*, 1998, **145**, 1882.
4. Q. He, S. Lv, Y. Huang, J. Guo, X. Peng, Y. Du and H. Yang, *Royal Society of Chemistry Advances*, 2023, **13**, 12464-12468.
5. L. Huang, Y. Chen, Y. Liu, T. Wu, H. Li, J. Ye, G. Dai, X. Zhang and Y. Zhao, *ACS Sustainable Chemistry & Engineering*, 2020, **8**, 17868-17875.
6. Y. Wang, Y. Huang, Y. Hua, Y. Du and H. Yang, *New Journal of Chemistry*, 2022, **46**, 14314-14317.
7. W. Ma, L. W. Luo, X. Huang, P. Dong, Y. Chen, C. Zhang, F. Huang, J. X. Jiang and Y. Cao, *Advanced Energy Materials*, 2022, **13**, 2203253.
8. X. Pan, P. Xue, X. Wang, F. Chen, Y. Gao, M. Tang, C. Wang and Z. Wang, *Chemical Engineering Journal*, 2022, **450**, 137920.
9. A. Duan, Z. Wang, X. Huang and Y. Li, *Angewandte Chemie International Edition*, 2023, **62**, e202302754.
10. H. Byeon, B. Gu, H.-J. Kim, J. H. Lee, I. Seo, J. Kim, J. W. Yang and J.-K. Kim, *Chemical Engineering Journal*, 2021, **413**, 127402.
11. G. Dai, X. Wang, Y. Qian, Z. Niu, X. Zhu, J. Ye, Y. Zhao and X. Zhang, *Energy Storage Materials*, 2019,

16, 236-242.

12. H. M. Li, T. T. Wu, Y. Y. Chen, Y. Liu, Z. Q. Jiang, X. H. Zhang, G. L. Dai and Y. Zhao, *Composites Communications*, 2021, **28**, 2452-2139.
13. F. A. Obrezkov, A. I. Somova, E. S. Fedina, S. G. Vasil'ev, K. J. Stevenson and P. A. Troshin, *Energy Technology*, 2021, **9**, 2000772.
14. F. A. Obrezkov, A. F. Shestakov, V. F. Traven, K. J. Stevenson and P. A. Troshin, *Journal of Materials Chemistry A*, 2019, **7**, 11430-11437.
15. J. Zhang, H. Liu, K. Jia, X. Li, X. Liu, L. Zhu, R. He and F. Wu, *Journal of Materials Chemistry A*, 2023, **11**, 2711-2717.
16. X. Zhao, X. Qiu, H. Xue, S. Liu, D. Liang, C. Yan, W. Chen, Y. Wang and G. Zhou, *Angewandte Chemie International Edition*, 2023, **62**, e202216713.
17. P. Acker, M. E. Speer, J. S. Wössner and B. Esser, *Journal of Materials Chemistry A*, 2020, **8**, 11195-11201.
18. Z. Niu, H. Wu, L. Liu, G. Dai, S. Xiong, Y. Zhao and X. Zhang, *Journal of Materials Chemistry A*, 2019, **7**, 10581-10588.
19. G. Dai, Y. Liu, Z. Niu, P. He, Y. Zhao, X. Zhang and H. Zhou, *Matter*, 2019, **1**, 945-958.
20. T. B. Schon, A. J. Tilley, C. R. Bridges, M. B. Miltenburg and D. S. Seferos, *Advanced Functional Materials*, 2016, **26**, 6896-6903.
21. W. Y. Ma, L. W. Luo, P. H. Dong, P. Y. Zheng, X. H. Huang, C. Zhang, J. X. Jiang and Y. Cao, *Advanced Functional Materials*, 2021, **31**, 2105027.
22. C. Li, J. Xue, A. Huang, J. Ma, F. Qing, A. Zhou, Z. Wang, Y. Wang and J. Li, *Electrochimica Acta*, 2019, **297**, 850-855.
23. K. Lee, I. E. Serdiuk, G. Kwon, D. J. Min, K. Kang, S. Y. Park and J. E. Kwon, *Energy & Environmental Science*, 2020, **13**, 4142-4156.
24. G. Dai, Y. Gao, Z. Niu, P. He, X. Zhang, Y. Zhao and H. Zhou, *ChemSusChem*, 2020, **13**, 2264-2270.
25. M. Kolek, F. Otteny, P. Schmidt, C. Mück-Lichtenfeld, C. Einholz, J. Becking, E. Schleicher, M. Winter, P. Bieker and B. Esser, *Energy & Environmental Science*, 2017, **10**, 2334-2341.
26. C. Zhao, Z. Chen, W. Wang, P. Xiong, B. Li, M. Li, J. Yang and Y. Xu, *Angewandte Chemie International Edition*, 2020, **59**, 11992-11998.
27. I. A. Rodríguez-Pérez, Z. Jian, P. K. Waldenmaier, J. W. Palmisano, R. S. Chandrabose, X. Wang, M. M. Lerner, R. G. Carter and X. Ji, *ACS Energy Letters*, 2016, **1**, 719-723.